

## Variable Responses of Equatorial Ionosphere During Undershielding and Overshielding Conditions

Debrup Hui<sup>1</sup>  and Geeta Vichare<sup>1</sup> <sup>1</sup>Indian Institute of Geomagnetism, Navi Mumbai, India

## Key Points:

- Distinctively different F region response to undershielding and overshielding prompt penetrating fields
- The top and bottom side F region starts showing strong gradients in plasma drifts as soon as overshielding commenced
- The thermospheric/ionospheric models cannot reproduce these altitudinal variations observed by radar

## Correspondence to:

D. Hui,  
debruphui@gmail.com

## Citation:

Hui, D., & Vichare, G. (2019). Variable responses of equatorial ionosphere during undershielding and overshielding conditions. *Journal of Geophysical Research: Space Physics*, 124, 1328–1342. <https://doi.org/10.1029/2018JA025999>

Received 15 AUG 2018

Accepted 14 JAN 2019

Accepted article online 18 January 2019

Published online 9 FEB 2019

**Abstract** This study tests the common assumption that the whole of the equatorial ionospheric *F* region responds uniformly to both undershielding prompt penetration and overshielding fields. Few recent studies have reported that the bottomside response to geomagnetic storms can differ significantly from that of the topside ionosphere. In this investigation, using vertical drift measurements from Jicamarca incoherent scatter radar in the altitude range of about 200 to 900 km, *F* region response to the space weather event on 9 November 2004 is studied. It is found that the *F* region showed large altitudinal variations in vertical drifts only under the influence of overshielding field. Such variations were negligible during undershielding prompt penetration conditions. In a first of its kind of study, direct observations of continuous altitudinal variations in vertical plasma drifts have been used to understand the response of *F* region ionosphere. This differential response to external drivers has a direct impact on the plasma transportations in the ionosphere and thus on estimating satellite drags. The observations are compared with the widely used ionosphere/thermosphere models: Thermosphere Ionosphere Electrodynamic General Circulation Model and Utah State University Global Assimilation of Ionospheric Measurements. It is found that contrary to observations, the Thermosphere Ionosphere Electrodynamic General Circulation Model shows very small altitudinal gradients in vertical drifts during both undershielding and overshielding conditions. Also, significant difference in the electron transportation especially at the bottomside between two models is adverted. Based on the observations, possible underlying physical processes of asymmetric interhemispheric potentials, different scale sizes of R1 and R2 current systems and different propagation modes for penetrating undershielding and overshielding fields are proposed.

**Plain Language Summary** The geomagnetic storms affect our transionospheric positioning, navigation, and communication systems by altering the transmitted radio signal. This alteration depends largely on plasma movement in the ionosphere. They can also create uncertainty in atmospheric drag calculation for Low Earth Orbital (LEO) satellites. Most of the models used for estimating these plasma movement assume or reflect that the ionosphere over equatorial region moves uniformly. Few recent studies, however, reported differential responses from topside and bottomside ionosphere. Knowledge about such complex ionospheric responses is critical for three-dimensional space weather models and estimation of accurate space weather effects on radio signals and satellite positions. Unfortunately, simultaneous observation of this nature from both topside and bottomside is difficult to make. In this study, we demonstrate how the incoherent scatter radar, located at Jicamarca Radio Observatory, Peru, can be very useful in making continuous measurements of storm time ionospheric changes from bottom to Low Earth Orbital satellite heights. This will improve our understanding of storm time changes in the ionosphere, which are not uniform as they are generally assumed to be.

## 1. Introduction

During geomagnetically disturbed time when interplanetary magnetic field's (IMF's) north-south component (IMF  $B_z$ ) turns southward, the motional interplanetary solar wind electric field (IEF) enters the Earth's ionosphere through the magnetosphere (Fejer et al., 1990; Nishida, 1968; Wolf, 1983). This penetration of electric field to the equatorial ionosphere from high-latitude ionosphere happens instantaneously and hence is referred to as prompt penetration (PP) electric field. When the Earth's ionosphere readjusts itself under the sudden penetration of incoming field from the outer magnetosphere, it is called undershielding condition. The reference to PP in the text will indicate this undershielding condition, unless stated otherwise. Over time, the inner magnetosphere develops an inertial field which opposes the incoming PP field producing shielding. When IMF  $B_z$  suddenly turns northward, withdrawing the penetrating IEF, the

inertial field dominates the ionosphere in the direction opposite to the original incoming field. This is generally referred to as the overshielding field (Gonzales et al., 1979; Kikuchi et al., 1996; Nishida, 1968). Both the PP and overshielding fields reach the equatorial ionosphere instantly imposing additional zonal electric fields in the opposite directions in dayside and nightside, respectively. This additional electric field gets superimposed on the tidal fields and modulates the plasma transportations over the equator. The tidal zonal electric field is eastward in the dayside, which drives the plasma upward, and westward in the nightside, which drives the plasma downward (Fejer, 1991, 1997; Scherliess & Fejer, 1999). The penetrating PP field is observed to enhance the eastward electric field up to around 2200 local time (LT) and induce westward field till morning hours (Fejer et al., 2008a). Another electric field associated with disturbed time, which influences the low to equatorial plasma transportation, originates from the changes in the neutral wind circulations in the subauroral thermosphere caused by the huge amount of energy deposited by storm time solar wind-magnetosphere-ionosphere-coupled processes. This is generally referred to as disturbance dynamo (DD; Blanc & Richmond, 1980) and becomes active from a few hours after PP electric field and lasts for up to a few days. DD is known to oppose the PP electric field over the equator (Fejer et al., 2008a).

The transmission of these penetrating fields has been studied for many decades by different instruments and models (Bhaskar & Vichare, 2013; Chakrabarty et al., 2017; Kelley et al., 2003; Nicolls et al., 2007; Nopper & Carovillano, 1978). The time delay for penetrating fields to reach low latitudes from high latitudes is of the order of a few seconds (e.g., Kikuchi et al., 1978, 1996), but their spatial distribution in three dimensions is difficult to study. This is because the ground-based individual instruments have very limited spatial coverage and, on the other hand, satellites can make very few localized in situ measurements in the timescales of these transient fields. Using a chain of magnetometers, an estimate of two-dimensional distribution of electric field can be made if the conductivity distribution is known ( $J = \sigma \cdot E$ ). But during disturbed time, the dynamics changes very fast and even the models can give only an approximation of the conductivities. Hence, it is very difficult to understand how these penetrating fields bring relative changes throughout the ionosphere. These transient electric fields dictate the plasma transportation/distribution during such disturbed periods. Over equatorial latitudes the horizontal magnetic field lines make it easier to estimate the electric field by measuring the  $\mathbf{E} \times \mathbf{B}$  plasma drifts. But ionosondes or coherent radars can mostly probe a small altitude range in the ionosphere. Incoherent Scatter Radars (ISRs), on the other hand, can probe much larger altitude range and give a very precise estimate of equatorial  $F$  region electric fields. Scherliess and Fejer (1999) and Fejer et al. (2008b) used extensive ISR measurements from the Jicamarca Radio Observatory (11.9°S, 76.8°W; dip latitude 1°N) and plasma drift data from the ROCSAT satellite, respectively, to understand the local time (or longitudinal) distribution of these vertical plasma drifts, which is a proxy for zonal electric field. In the off-equatorial region, where magnetic field lines are not parallel to the ground, the tidal and midlatitude winds control the dynamo and thus affect the value of the  $\mathbf{E} \times \mathbf{B}$  drifts (Fesen et al., 2000; Liu et al., 2013; McLandress et al., 1996; Patra et al., 2014, and references therein). While using Jicamarca ISR measurements, however, data are altitudinally averaged around the height of peak density region to get the best signal-to-noise ratio (SNR). But in doing so, the altitudinal variations in the plasma drifts get neglected and that, in turn, violates the basic curl-free condition of electric field in the ionosphere. Murphy and Heelis (1986) show that to satisfy the basic curl-free condition of electric fields, which connects the longitudinal gradients of vertical electric field with the altitudinal variations of zonal electric field, the vertical plasma drifts change with altitude. These quiet time altitudinal variations have been studied by Pingree and Fejer (1987), Fejer et al. (2014), and Hui and Fejer (2015). It has been shown that the altitudinal gradients in vertical plasma drifts are small during the day and postmidnights (Pingree & Fejer, 1987) but can become considerable across the sunset terminator (see Fejer et al., 2014). However, it remains almost unaddressed as to how the penetrating fields (which modify the quiet time plasma transportations) affect the altitudinal variations of the plasma drifts during disturbed times. To address this question, in this study, we have used Jicamarca ISR data from a disturbed time event on 9 November 2004 and show the effects of undershielding and overshielding fields on vertical plasma drift variations with height. During this event, very distinctive changes in the altitudinal patterns of the vertical drifts are observed under the influences of different penetrating fields. Because the higher-altitude field lines connect to higher latitudes, these variations also reflect the latitudinal variations of zonal electric field along the low latitudes away from the equator. So it is very interesting to see that the radar captured very distinctly different  $F$  region response to both penetrating fields. Moreover, many recent studies compared  $F$  region

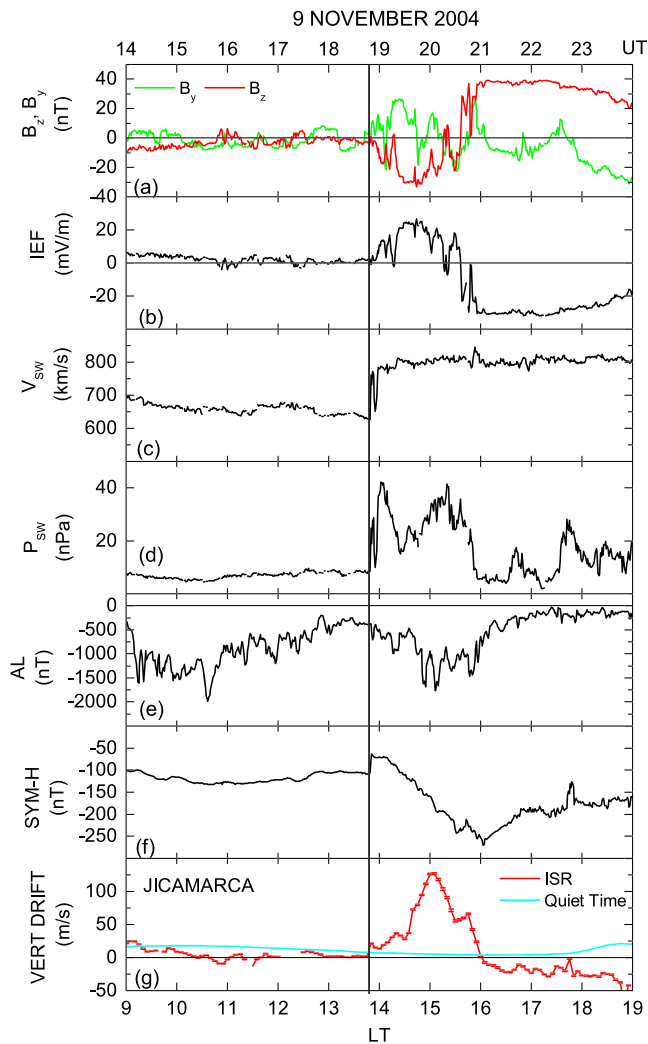


**Figure 1.** Solar wind, magnetospheric, and drift measurements for the event on 9 November 2004. From top are (a) IMF  $B_z$  and  $B_y$ , (b)  $IEF_y$ , (c) solar wind velocity, (d) solar wind pressure, (e) AL index, (f) SYM-H, and (g) vertical plasma drifts measured by Jicamarca ISR along with Scherliess and Fejer, (1999) model drift values in cyan. (LT = UT - 5: both UT and LT are mentioned at top and bottom axes, respectively).

bottomside response with topside response to disturbed time drivers (Astafyeva et al., 2016; Pedatella et al., 2009; Yizengaw et al., 2006). They found, using satellite and complimentary ground observations, very different to opposite responses from bottomside and topside ionosphere. It is emphasized that such observations are very challenging because of unavailability of complimentary data sets or a single instrument to make such observations. The present study also demonstrates how Jicamarca ISR can be very effectively used for continuous monitoring of such complex  $F$  region responses. In addition, to test and validate our present understandings, we then compared the observed variations during the space weather event of 9 November 2004 with simulation results from Thermosphere Ionosphere Electrodynamic General Circulation Model (TIEGCM) and Utah State University Global Assimilation of Ionospheric Measurements (USU-GAIM) model runs for the event. It was found that during both undershielding and overshielding times, the model produced patterns which are different from the radar observations. Understanding the source of these altitudinal variations and incorporating them in the model is critical to the knowledge of 3-D ionospheric electrodynamic. These variations have a direct impact on the drag estimations for low Earth orbital (LEO) satellites.

## 2. Data and Observations

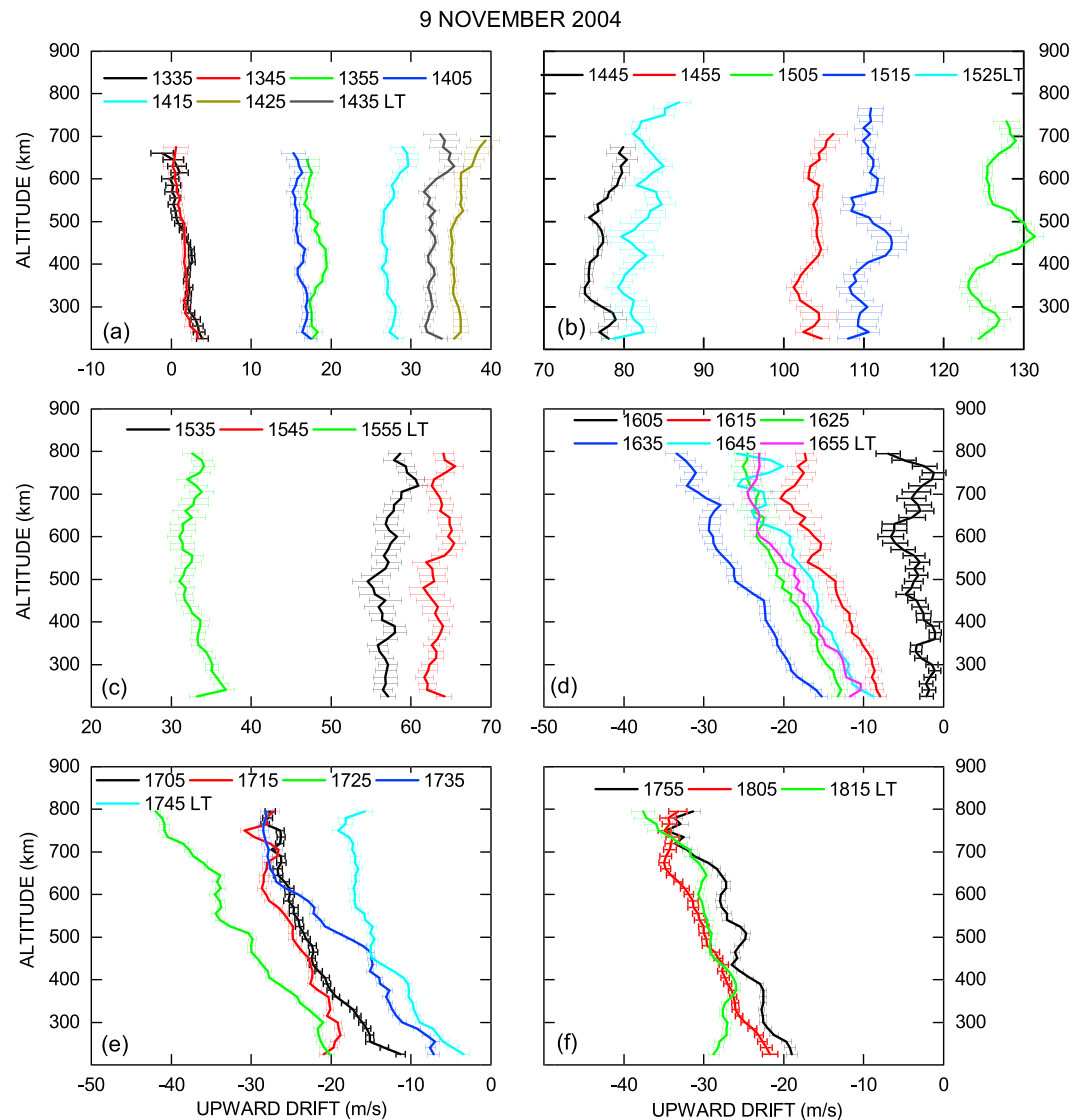
To get an insight into the altitudinal variations in the  $F$  region ionosphere due to penetrating fields, this study uses vertical plasma drift data from the ISR at Jicamarca, Peru, recorded during the space weather event on 9 November 2004. To support the analysis, solar wind parameters and geomagnetic indices are taken from National Aeronautics and Space Administration Coordinated Data Analysis web and Kyoto World Data Center for Geomagnetism, respectively. When the vertical plasma drift data have an altitudinal resolution of 15 km and a temporal resolution of 5 min, the solar wind and geomagnetic indices have 1-min resolution. The Jicamarca ISR measures plasma drifts in the  $F$  region with very high accuracy. The measurement techniques and in-depth details about the Jicamarca ISR can be found in Fejer (1997) and Kudeki et al. (1999). A good SNR exists from 200 km to around 500 to 900 km depending on the solar flux conditions. A higher solar flux produces higher ionization at larger altitudes, making the ionosphere expand, thus giving higher SNR on the topside. Because of the unique location and geometry of the geomagnetic field, the Jicamarca ISR makes

the most accurate estimates of electric fields in the equatorial ionosphere (Kelley et al., 2003). The data used here from the ISR have measurement errors of less than 2 m/s at all altitudes considered.

The geomagnetic storm of 8 to 12 November 2004 is one of the strongest geomagnetic storms (SYM-H < -270 nT) in the solar cycle 23 and has been widely studied (e.g., Deng et al., 2009; Fejer et al., 2007; Tsurutani et al., 2008). When numerous studies have already reported different aspects of this storm, this study will try to focus on the effects of penetrating electric fields on altitudinal variations in vertical plasma drifts. Figure 1 shows the variations in solar wind parameters, geomagnetic indices, and Jicamarca radar data for the space weather event of 9 November 2004. From the top, panels show IMF  $B_z$ /IMF  $B_y$ , the east-west component of IEF ( $IEF_y$ ), solar wind velocity ( $V_{sw}$ ), solar-wind pressure ( $P_{sw}$ ), auroral electrojet index (AL), ring current index (SYM-H), and vertical plasma drift measured by ISR. Though the primary focus of this study spans from about 1850 UT to about 2300 UT (1350 LT to 1800 LT) encompassing the undershielding phase of the storm (main phase after IMF  $B_z$  turns southward at around 1850 UT) to overshielding (after around 2043 UT, when IMF  $B_z$  turns northward), some history has been included to impress upon the fact that before the main phase, IMF  $B_z$  was almost steady for a long time with small negative value.

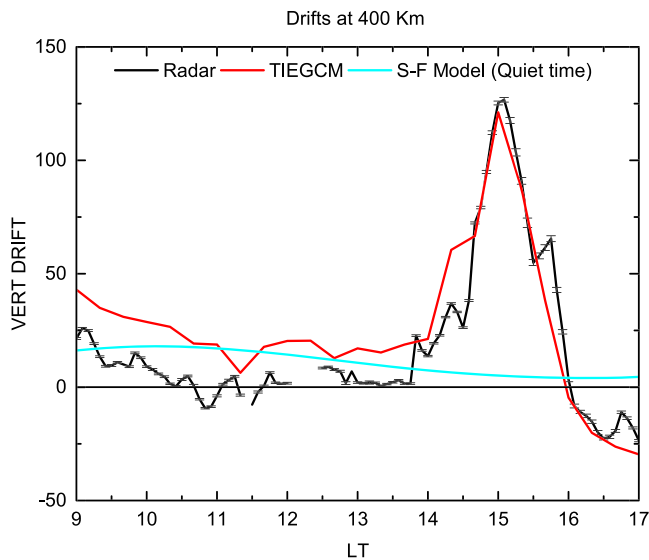
Accordingly SYM-H was also steady at about  $-100$  nT because of the disturbances from the previous day. The IMF  $B_z$  started intensifying fast from about 1850 UT and within a few minutes reached a value of about  $-20$  nT. With two brief oscillations, it reached a value of about  $-30$  nT by 1930 UT. From about 1945 UT it started decreasing and recorded two instances of reduced intensity. The second of the two decreases exacted IMF  $B_z$  northward for a brief period before another quick intensification to about  $-23$  nT. Finally, at about 2043 UT it turned northward giving rise to overshielding condition. The IEF<sub>y</sub>, which is derived from the product of IMF  $B_z$  and  $V_{sw}$  and maintains an anticorrelation with IMF  $B_z$  is shown in Figure 1b. Figures 1c and 1d show the solar wind velocity,  $V_{sw}$  and pressure,  $P_{sw}$ , respectively. At around 1850 UT, when the very slowly changing solar wind velocity jumped suddenly from 630 to 760 km/s, the pressure jumped from a steady value for a long time of about 7–8 nPa to about 30 nPa. Figure 1e shows the high-latitude AL index, which shows enhanced activity reaching up to about 1,800 nT during peak IMF  $B_z$  intensity. This intensification of AL is expected due to the strong earthward convection-related electric field changes and/or particle precipitations in the high latitudes. Figure 1f shows the SYM-H index and records a Storm Sudden Commencement (SSC), which should coincide with the pressure jump at about 1850 UT. It is important to mention that when the time series of the solar wind parameters shifted to the bow shock nose (time-shifted data from OMNI/CDA web) are compared with ground-based SYM-H index, it was found that the SSC in SYM-H does not coincide with the sudden increase in the  $P_{sw}$ ; rather, the time delay is overestimated by 6 min. Therefore, a time correction of 6 min to align the SSC observed in SYM-H with the jump in solar wind pressure at about 1850 UT is applied to all the solar wind parameters (IMF, IEF<sub>y</sub>, and  $P_{sw}$ ). It can be noted from the plots that the SSC also marks the beginning of southward intensification of IMF  $B_z$  and storm main phase. Figure 1g shows the height-averaged vertical plasma drift data from 300- to 500-km altitude. The jump in pressure is expected to cause enhanced eastward electric field on the dayside ionosphere (Huang et al., 2008). The drifts, expectedly, start to increase as soon as  $P_{sw}$  increases, and then overtaken by southward turning of IMF  $B_z$ , and reaches a peak value of about 127 m/s at around 1505 LT (2005 UT). The drift then starts decreasing with weakening IMF  $B_z$  values and reverses to downward direction at around 1605 LT, soon after SYM-H started recovering. It is important to note that the ionospheric changes due to the prompt penetration fields show some delay of up to 13 min on average (Ridley et al., 1998) as will be discussed later. When this delay is not very clear at the beginning of the main phase probably because of the superimposed effects of  $P_{sw}$  and IMF  $B_z$ , it can be clearly noticed when IMF  $B_z$  turned northward. So from about 1543 LT to 1605 LT, when IMF  $B_z$  was northward and fluctuating before becoming steady, the ring current continued to intensify and SYM-H reached a peak value of  $-271$  nT at 1603 LT (2103 UT). The westward overshielding field due to northward turning of IMF  $B_z$  seems to affect vertical drifts from 1600 LT onward. It is to be noted that the vertical plasma drifts have a 5-min temporal resolution against 1 min of SYM-H. Also, plotted in cyan is the climatological quiet time model drift values from the Scherliess-Fejer model (Scherliess & Fejer, 1999). It can be noted that the disturbed time drifts differ significantly from the quiet time values.

Figure 1 shows that the drifts turned downward coinciding with the starting of the recovery phase in the SYM-H index. Before the storm, the SYM-H was steady at about  $-100$  nT because of the disturbances from the previous day (not shown here). Therefore, DD effects are expected to superimpose on the tidal fields before and during the storm period. However, during the main phase, PP electric field effects are dominant, while overshielding effects are prominent during the recovery phase. Hence, the plasma transportation would be primarily driven by tidal field affected by DD field before the main phase whereas prompt penetration field would dominate during the main phase. After IMF  $B_z$  turned northward, overshielding field would primarily drive the plasma transportation. Figure 2 captures the altitudinal variations in vertical plasma drifts over Jicamarca during these different phases with a time resolution of 10 min. The legends mark the midpoint of the time ranges. Each profile has three-point running altitudinal average to filter out high-frequency fluctuations. The drift profiles, for easy comparison, have been put in different panels so as to accommodate the huge range of drift values without changing the scaling. This makes it easier to compare between different panels. The error bars represent the measurement uncertainty. It can be seen that before the main phase started, the altitudinal variations are very small. Though not strictly quiet (SYM-H  $\sim -100$  nT), no large transient field is present at least few hours before the main phase. The altitudinal variations during this time are similar to the variations during geomagnetically quiet time afternoon hours and this season, when the vertical drifts decrease very slowly with altitude (Hui & Fejer, 2015). For instance, in Figure 2, before the main phase started (1335 LT, 1345 LT), the drifts slowly decrease from 5 m/s at around



**Figure 2.** Altitudinal variations of vertical plasma drifts before the storm, during undershielding (a-c) and overshielding (d-f) conditions. Each vertical profile is the average of 10-min data.

200 km to 0 m/s at 700 km at an almost linear rate of  $-0.01$  m/s/km. As the main phase starts after 1350 LT, and the drift values start increasing, the altitudinal variations remain very small or at times (e.g., at 1445 LT, 1455 LT) slightly increase with altitude. The drift value maximizes at around 1505 LT as can be seen in panel 2b and then starts decreasing before turning downward at around 1605 LT in panel 2d. What is of prime importance here is that before turning downward, the altitudinal variation of drifts in panels 2a–2c are very small, but as soon as the drifts turned downward, very strong altitudinal variations can be seen with the topside drifts decreasing much faster than the bottomside (panel 2d). This trend continues till panel 2f and beyond. The downward drifts vary from about 15 m/s at 200 km to about 35 m/s at 800 km showing a stronger gradient of  $-0.03$  m/s/km at 1635 LT. The strongest variation, of the order of  $-0.04$  m/s/km, is probably seen at 1725–1735 LT, about 100 min after overshielding started. It can be noted that the bottomside downward drifts remain less than about 20 m/s, whereas the topside drifts reached values of up to  $-42$  m/s. This indicates a very strong altitudinal gradient as soon as overshielding started dominating, which is very different from the main phase or before the storm started. This differential response of the F region forms the central theme of this study, which is rarely observed. It is important to note that from 1445 LT to 1505 LT, some wave-like structure seems to propagate, which slowly



**Figure 3.** Comparison of TIEGCM drift values with Jicamarca ISR measurements at 400 km.

diminishes down in the following 20-min interval. The vertical wavelength is found to be  $\sim 200$  km in 1505 LT profile, which is too large to be gravity waves. The source and nature of the observed wave-like activity, though very interesting, are beyond the scope of the present work and will not be discussed further in this study.

## 2.1. Comparison With Models

To check if the widely used models can reproduce or indicate toward such physical changes in the ionosphere, we have evaluated the event using two popular ionospheric models: TIEGCM and USU-GAIM models. Note that TIEGCM is a general circulation model which solves full three-dimensional dynamical thermospheric wind equations, whereas USU-GAIM is an assimilative model.

The National Center for Atmospheric Research TIEGCM is a first-principle, nonlinear, self-consistent 3-D thermosphere-ionosphere model which gives low-latitude plasma drifts as one of the outputs. The model uses three-dimensional momentum, energy, continuity equations for numerous ions, and neutral species. The model uses  $5^\circ \times 5^\circ$  latitude-longitude grids as default simulation settings and 29 constant pressure levels in the vertical direction covering from 97 to about 500 km. The model takes 10.7-cm solar flux, high-latitude electric potentials from

Heelis et al. (1982) or Weimer (2005) as inputs, and on the bottomside it takes diurnal and semidiurnal migrating tides specified by Global Scale Wave Model (GSWM; Hagan & Forbes, 2002). More details about the model can be obtained from Dickinson et al. (1981), Qian et al. (2014), Roble et al. (1988), and Richmond et al. (1992), and references therein. The model has been tested successfully for many important ionospheric processes like storm time electrodynamic changes, composition changes, and postsunset vortex in plasma flow (e.g., Hagan et al., 2007; Qian et al., 2009; Vichare & Richmond, 2005).

The USU-GAIM is a physics-based assimilation model. It is based on the global Ionosphere Forecast Model (IFM) covering from around 90 to 1,400 km and a Kalman filter to assimilate a diverse set of real-time ionospheric data from all over the globe. Along with the primary output of time-dependent three-dimensional electron density distribution, it gives distribution of different important ions in the global ionosphere. IFM takes 10.7 solar flux,  $A_p$ ,  $K_p$  indices, and empirical neural and magnetospheric parameters as inputs. The latitudinal and longitudinal resolutions are  $4.66^\circ$  and  $15^\circ$ , respectively. More details about the model can be obtained from Schunk et al. (2004) and Scherliess et al. (2006).

The TIEGCM run for the event was made from 00:00 UT to 24:00 UT for 9 November 2004 with default resolution of the model which is  $5^\circ$  longitudinal (spatial) and 20-min temporal resolution. The high-latitude potentials which go as input to estimate the magnetospheric energy entering in to the high-latitude ionosphere was used from Weimer (2005). The first thing that is being compared is the drift values at a representative height of 400 km as the storm develops. This is shown in Figure 3. The model output at 400 km is plotted against the altitudinal average radar measured vertical plasma drifts in the altitude region of 380 to 420 km over Jicamarca. Also shown is the quiet time Scherliess and Fejer (1999) model values. As can be seen from the figure that although before the main phase the model overestimates the drift, it successfully reproduces drift values that match very well with the observations as the storm progresses. What is interesting here is that the peak value of about 127 m/s occurs very rarely during intense storms over Jicamarca, which the model reproduced very closely.

Having noted that the model produces measured values quite closely, Figure 4 shows the altitudinal variations in vertical plasma drifts before the main phase, during main phase, and during overshielding periods from TIEGCM run. To accommodate the large range of drift values, the panels in Figure 4 have been readjusted so as to make the  $X$  axis scaling match from one panel to another. Each vertical profile has a time resolution of 20 min. During the main phase, the TIEGCM run produced the drift values up to about 660 km. The altitudinal variations before the starting of the storm were very small, as can be seen in panels 4a and 4b. The model shows that the altitudinal variations in the  $F$  region increased during the main phase (see

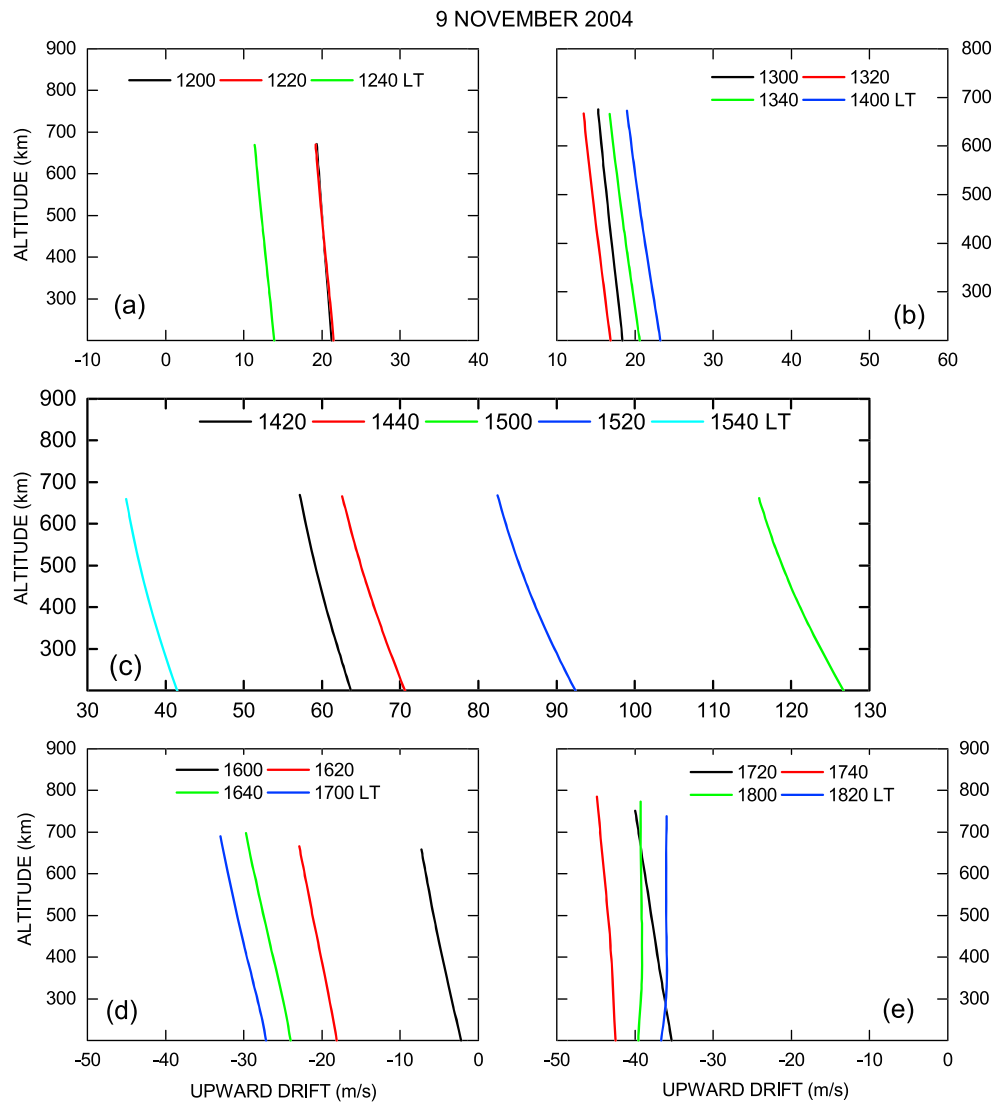


**Figure 4.** Altitudinal variations of vertical drifts reproduced from TIEGCM run during different phases of storm. Panels (a-b) show vertical profiles of drifts before and at the beginning of the storm, (c) during the main phase and (d-e) during overshielding.

panel 4c) with drifts slowly decreasing with altitude and the variation intensifying as the storm progresses or IMF  $B_z$  maximizes. The highest gradients are seen at around 1500–1520 LT. For instance, at 1500 LT, the bottomside (200 km) shows a drift of about 127 m/s and slowly decrease to 116 m/s at 661 km giving a linear gradient of  $-0.02$  m/s/km. As soon as the drifts turned downward and overshielding starts dominating at around 1600 LT, the altitudinal variations become smaller (panel 4d) and by 1800 LT, they even show reverse trend: drift increases with altitude (see panel 4e). Thus, from the model run, it is observed that the altitudinal variations in vertical plasma drifts are maximum during peak main phase of the storm and are considerably smaller before the storm and during overshielding. Further comparison of results from both models is done in the discussion section.

### 3. Discussions

The altitudinal variations of vertical plasma drifts exist during quiet times to satisfy the curl-free nature of the electric field. The longitudinal gradients of zonal plasma drifts are proportional to altitudinal gradient of vertical plasma drifts (Murphy & Heelis, 1986). Using Jicamarca ISR data during moderate solar flux

conditions, Pingree and Fejer (1987) have validated this relationship. As stated earlier, mostly Jicamarca data are averaged over altitudinal range around the peak density altitude where SNR is maximum. But in doing so, the altitudinal variations are neglected. In a 3-D ionospheric electrodynamic model, such altitudinal variations are important as they reflect the latitudinal structures of ionospheric electric field away from the equator. The higher altitudes are electrodynamically connected by flux tubes to higher latitudes. Flux tubes or magnetic field lines have very high parallel conductivity and hence considered equipotential. So any strong altitudinal structure in vertical plasma drifts would indicate strong latitudinal variations in zonal electric field. These variations in low-latitude electric field have a direct effect on the plasma transportation in the low-latitude to equatorial ionosphere. During geomagnetically disturbed times, however, different external electrodynamic drivers of solar wind or magnetospheric origin penetrate the global ionosphere. When effects of many restricts to high latitudes, (e.g., particle precipitation, Polar Boundary Intensifications, etc.), few of them penetrate down to equatorial latitudes, such as undershielding prompt penetration electric fields, overshielding (e.g., Kelley et al., 2003; Nopper & Carovillano, 1978), and storm time substorm-induced electric fields (e.g., Hui et al., 2017). These external drivers along with the DD mentioned earlier can dictate the plasma distribution in the ionosphere. Some recent studies (Astafyeva et al., 2016; Pedatella et al., 2009; Yizengaw et al., 2006) have been carried out on the topside and bottomside differences in the  $F$  region during such disturbed times. These studies suggest that during storms, the top and bottomside can show different, even opposite response under the influence of different drivers, which can be combinations of penetration fields, DD, changes in thermospheric winds, and composition. For topside response, such studies mostly depend on satellite data, which is hard to find at certain regions and at any specific times to be complimented with available ground-based bottomside observations. Astafyeva et al. (2016) observed that the lack of such instruments which can observe or monitor both bottomside and topside simultaneously is crucial but difficult to find. In this study, we demonstrate that the altitudinal variations in vertical plasma drifts measured by the Jicamarca ISR provide a very good platform for continuous monitoring of such differences up to about 600–900 km (connecting up to  $\sim 22^\circ$  geomagnetic latitudes) subject to solar flux conditions. This can provide a great insight into how the external drivers bring about modifications in the equatorial to low-latitude ionosphere, especially during disturbed times. It is suggested from observations (e.g., Fejer, 1986; Sastri, 1988) and theoretical models (Kikuchi et al., 1978, 1996) that the penetrating fields affect the global ionosphere (from high latitudes to low latitudes) in timescales of few seconds; and their local time variations are known to a great extent (Fejer et al., 2008a, and references therein). But how the external drivers modify the altitudinal variations of vertical plasma drifts over equatorial and low latitudes is rarely addressed. In this event-based study, for the first time, we show that the disturbed time external fields can result in large altitudinal variations in vertical plasma drifts, which are difficult to explain using the disturbed time changes in the thermospheric neutral winds in timescale of few minutes. We also demonstrate that the popular models fail to reproduce the observed altitudinal variations under the influence of these external fields.

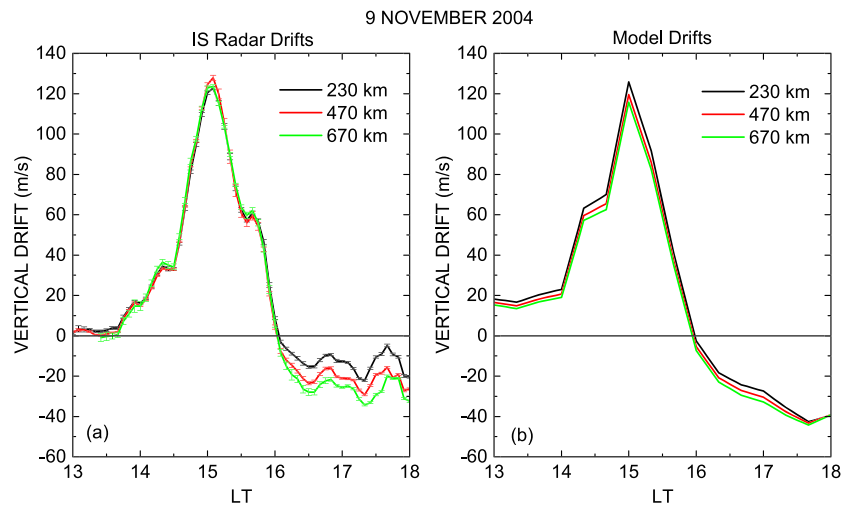
The Jicamarca ISR is the most accurate instrument for estimating equatorial ionospheric electric fields, better than in situ measurements with an accuracy of  $25 \mu\text{V/m}$  (Kelley et al., 2003). During solar minimum, when the ionosphere is shallow, it can make good measurements up to 500–600 km whereas during solar maximum, the ionosphere expands and reliable measurements can be made up to 800–900 km. The event on 9 November 2004 occurred when solar flux was moderately high with 10.7 cm solar flux index of 138. Before the storm, the topside data was noisy above 700 km but during the main phase of the storm, very good SNRs were recorded up to 800–900 km with error values  $\leq 2$  m/s. So, it can be safely concluded that the drift measurements presented in this study are of high reliability.

Figure 1 shows that the event of southward component of IMF  $B_z$  intensifying and then turning northward took place in a span of about 2 hr: 1350 LT to 1543 LT (1850 UT to 2043 UT). It is one of the fastest and strongest intensification in solar cycle 23 when the IMF  $B_z$  value reached up to  $-30$  nT and then recovered. The resultant vertical drift recorded by the Jicamarca ISR reached up to 127 m/s equivalent to a zonal electric value of about 3.17 mV/m over Jicamarca. Such large value is very rare (Fejer et al., 2007) and is expected to cause a super fountain effect (Tsurutani et al., 2004, 2007) which would take the  $F$  layer plasma at much higher altitudes than usual. With the  $F$  layer ascending fast, the ISR captured very good signal from the topside due to enhanced topside density. In fact during the main phase, SNR data shows that the  $F$  peak layer moved from around 450 km at 1435 LT to 575 km at 1505 LT and to about 725 km at 1535 LT. It is important to note that during the start of main phase, the enhancement in eastward electric field may have been

assisted by the dayside compression because of the sudden jump in solar wind pressure (Huang et al., 2008). During this event, even though IMF  $B_z$  turned northward at 1543 LT, the SYM-H continued to intensify, indicating continued convection in the magnetosphere. This resulted in delayed penetration of overshielding fields by about 17 min (1543 LT to 1600 LT) until SYM-H started recovering and vertical plasma drifts became negative. Such delay in penetration of prompt penetration field is possible as shown by many studies (e.g., Bhaskar & Vichare, 2013; Ridley et al., 1998, and references therein) to account for different transmission times from the bow shock to the ionosphere through the magnetosphere. Northward turning of the IMF  $B_z$  marks the dominance of overshielding field and consequently the ionosphere starts descending under the influence of westward penetration field.

The vertical plasma drift shown in Figure 1 is the altitudinal average from 300 to 500 km. But the actual measured drifts varied with altitudes as shown in Figure 2. As has been mentioned before, the altitudinal variations before the main phase is very small and similar to the quiet time afternoon altitudinal variations as shown in climatological study by Hui and Fejer (2015). With the start of main phase, as can be seen in Figure 2, the whole of the  $F$  region gets affected in the same manner (the upward drift enhances) showing very small altitudinal variations before and during the main phase. These small altitudinal variations during main phase indicate very weak latitudinal variations in the zonal component of ionospheric electric field and are consistent with the observations of Fejer et al. (1990). Overshielding field on northward turning of IMF  $B_z$  also penetrates in a matter of few seconds from high latitudes down to equatorial latitudes. But on this particular event, as soon as convection started weakening and SYM-H started recovering, the topside downward drifts seem to increase much faster than the bottomside drifts. Very large downward drifts can be seen at the topside compared to the bottomside  $F$  region. This steady character in altitudinal variations soon after triggering of overshielding field is also reflected in the time series data of drifts shown in Figure 5a. Drifts at various altitudes have been compared and it can be clearly seen that as soon as westward field starts dominating, driving downward vertical drifts, higher altitudes consistently maintained larger downward drifts compared to lower altitudes. In other words, higher altitudes experienced much stronger westward electric field values than the lower altitudes. These altitudinal variations in drifts are much larger than the quiet time afternoon values observed by Hui and Fejer (2015). For example, during November-December, at around 1600 LT, vertical plasma drifts show a very weak gradients of about  $-0.007$  m/s/km from 200- up to 650-km altitude. In contrast, the drifts seen during this event are about  $-0.03$  m/s/km at 1635 LT and about  $-0.04$  at 1725 LT, which are an order higher than quiet time climatological values. As mentioned earlier in the previous section, TIEGCM simulation results for this event displayed in Figure 3 show that before the storm the altitudinal variations are very small, increases by a small value around the peak of the main phase, and then reduces as storm ends. The drifts are almost height independent or even tend to start increasing with altitude from around 1800 LT. The time series data from model at different altitudes are shown in Figure 5b next to the radar observations for comparison. The model could reproduce the magnitudes close to the observations during the main phase, but not the altitudinal variations, particularly in the recovery phase.

These altitudinal variations over the equator during the overshielding phase may indicate very important effects on the plasma transportation at different altitudes and latitudes. It means that the plasma at higher altitudes would come down faster than the plasma at lower altitudes. During main phase the PP electric field would take the plasmas to much higher altitudes and then move along the field lines to the higher than usual equatorial ionization anomaly peak latitudes, resulting in the super fountain effect (Tsurutani et al., 2004, 2007). But as soon as westward (overshielding) electric field dominates, the plasma will start moving toward the equator because of the westward field (or the downward drift). So under the PP electric field the plasma will be expected to rise and reach higher low latitudes along the field line, and under overshielding the Equatorial Ionization Anomaly plasma density peak is expected to move equatorward. According to our observations, during the recovery phase, the downward drift values are larger at higher altitudes compared to that at the lower heights. As the higher apex height or higher latitude experience stronger westward field, plasma crossing these flux tubes would be expected to descend faster than the plasma crossing the lower apex height flux tubes over the equator connecting the lower latitudes. We carried out simulation using both TIEGCM and USU-GAIM to find out the plasma transportation from equator to higher latitudes under PP electric field and reverse during overshielding fields. When both models showed fountain effect, the peak plasma height over the equator did not reach as high as observed by the radar. The radar data show that the  $F$  region peak moved up to 765 km at around 1555 LT, just before the descent started.



**Figure 5.** Local time variations of vertical drifts as observed by Jicamarca ISR (a) and modeled drifts from TIEGCM run (b). The ISR drifts have three-point running average to reduce high-frequency fluctuations.

The latitudinal distribution of electron density at different altitudes is shown in Figure 6 from both models. In the figure, density profiles are shown for every 20 min for TIEGCM whereas for every 15 min for USU-GAIM from 1500 LT to 1700 LT (2000 UT to 2200 UT). The different time resolutions are the default output resolutions of the respective models. When TIEGCM run showed peak density region at around 15° geomagnetic latitude and at around 500-km altitude, USU-GAIM showed anomaly crest region at about 15° geomagnetic latitudes and at 300 km. Also notice that from 1500 LT to 1600 LT, when the PP electric field was acting, TIEGCM peaks both at 500 and 700 km moved further away from the equator and thereafter started moving equatorward under the influence of overshielding effect. No such features were observed in USU-GAIM-generated electron distributions, probably because of the coarse longitudinal resolution (15°) of the model. The density estimates also differed greatly between the two models: at 300 km, USU-GAIM showed an order of magnitude more density than TIEGCM; at 500 km the density estimates are twice of that of TIEGCM, whereas at the topside they are comparable. TIEGCM is a first-principle physics-based model, whereas USU-GAIM is a very effective plasma transportation model which incorporates thousands of global measurements. That is why both models are being used to investigate a comparison of plasma transportation between them during a unique observation of the ionosphere. It may be an indication that the first-principle model is missing very crucial storm time physics or the data assimilation techniques need to be looked carefully.

The variations in plasma drift velocities indicate the differential rate of plasma transportation in the low-latitude ionosphere, which can have very serious effect on LEO satellite experiencing atmospheric drag in the lower equatorial ionosphere. The storm time fountain effect moves the ionospheric plasma which drags the neutrals along with them to higher altitudes thus producing uncertainties in satellites positioning (e.g., Tsurutani et al., 2007). The accuracy of satellite positioning and the probability of collisions even using high end algorithms can degrade because of the uncertainties in densities (see, e.g., Bussy-Virat et al., 2018). When many previous storm time observations have noticed the differential *F* region response from bottomside to topside, no clear understanding or methodology has emerged. In this study, we observed strong altitudinal difference from bottomside to topside indicating latitudinal variations in storm time electric field. This would result in faster collapsing of plasma in the outer (higher altitudes/latitudes) flux tubes than the inner (lower altitudes/latitudes) ones. This would result in the accumulations of plasmas at certain altitudes/latitudes which would be different if whole of the *F* region moves with same drift values. This response of the ionosphere to the external driver is very intriguing.

The altitudinal gradient of vertical plasma drifts depends on the longitudinal gradients of zonal plasma drifts, which are significant around sunset terminator. In fact, on this day, initiation of pre-reversal enhancement (PRE; e.g., Eccles, 1998; Fejer et al., 2014) of zonal electric field can be seen in the bottomside drift data at around 1820 LT. But the differential response of the *F* region being discussed here started at around 1600

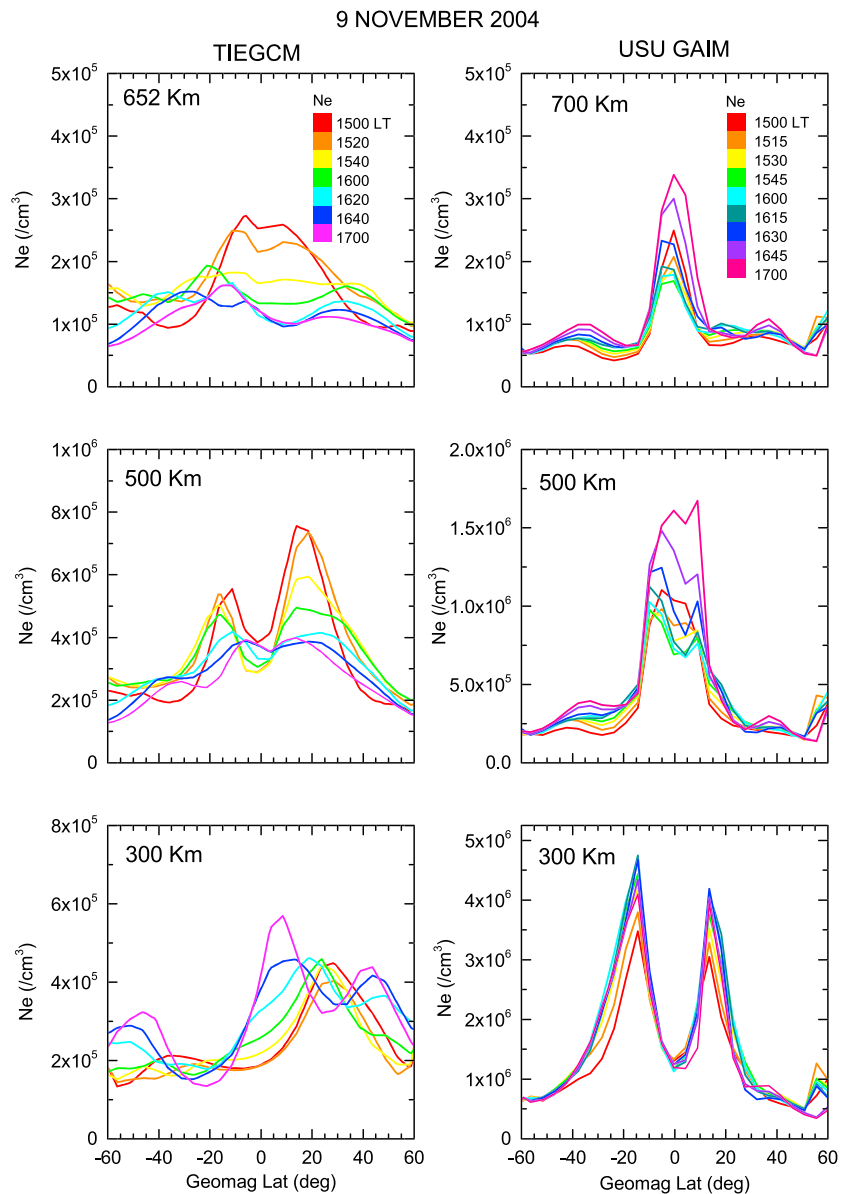


**Figure 6.** Latitudinal distribution of plasma density from (left) TIEGCM and (right) USU-GAIM model runs at different altitudes.

LT, much before the time when longitudinal gradients become stronger. So any influence from the PRE can be ruled out as a reason for the observed gradients. Interestingly, the altitudinal gradients appeared with the IMF  $B_z$  turning northward which is also accompanied by sudden decrease in solar wind dynamic pressure,  $P_{sw}$ . The increase in  $P_{sw}$  at around 1350 LT and decrease at around 1550 LT are expected to induce eastward and westward zonal electric fields, respectively, over Jicamarca. But any role of solar wind pressure in creating such altitudinal gradients is least likely, because if decrease in solar wind pressure is the reason to create the sudden altitudinal gradients, then in the main phase soon after increase in dynamic pressure, also a gradient would be expected.

Deng et al. (2009) showed that, during this event, the polar convection patterns reversed as IMF  $B_z$  turned strongly positive and within 45 min because of ion-neutral momentum exchange, a reverse neutral wind convection was set up. During such strongly positive IMF  $B_z$  and high solar wind pressure, reconnection takes place at the high-latitude magnetosphere (Crooker, 1992; Song et al., 1990), which can give rise to very complex convection patterns in high latitudes with sunward flow over polar region (Burke et al., 1979) and

replacing the well-known DP2 convection during southward IMF  $B_z$  (e.g., Chakrabarty et al., 2017). When a strongly northward IMF  $B_z$  condition exists for ion-neutral momentum exchange time constant of few hours, neutrals start mimicking the ion convection (Deng et al., 2009; Killeen et al., 1985; Rishbeth, 1977, and references therein). Deng et al., (2009) observed an altitude-dependent reverse neutral convection over high latitudes after at least 45 min of northward turning of IMF  $B_z$ . Such changes in high-latitude wind are expected to cause some secondary changes in the middle- and low-latitude ionospheric electric fields (Richmond et al., 2003) but with a time delay of few hours. Hence, any changes in altitudinal gradients of vertical drifts recorded by the Jicamarca ISR because of this reverse convection is least likely. On the other hand, DD electric fields take 1–3 hr to reach equatorial latitudes (Fejer, 2011; Fejer et al., 2017; Zhang et al., 2017) and are usually small at this local time sector (Fejer et al., 2008a). When the storm time wind changes from higher latitudes and its interaction with the DD present due to previous day's disturbances can possibly make substantial changes in the equatorial ionosphere after the commencement of the storm activity (about 2 hr), such interactions fail to explain why the altitudinal variations changed suddenly as soon as overshielding is triggered.

The observed altitudinal gradients indicate a strong latitudinal gradient in the potential distribution, but as discussed earlier, during disturbed times, the latitudinal variations in electric field is generally weak (Fejer et al., 1990). During southward IMF  $B_z$ , the potential distributions are driven by the DP2 convections but as IMF  $B_z$  turns northward, the polar cap convection patterns changes drastically making changes in the potential distribution patterns (see Figure 3 in Deng et al., 2009). This change of potential mainly driven by the shielding effect of R2 current system could possibly escalate the hemispherical asymmetry already existing because of asymmetry in nondipolar magnetic field components and Sq potential resulting in large potential differences at both ends of the flux tubes. If the zonal gradients of these potentials follow certain latitudinal patterns, one can expect such gradual changes in the zonal electric fields with changing altitudes. In case of hemispherical asymmetry, if the azimuthal potential gradients changes differently in opposite hemispheres, the nature of altitudinal gradients can get more complicated. Many recent studies (e.g., Astafyeva, Zakharenkova, & Doornbos, 2015; Astafyeva, Zakharenkova, & Förster, 2015; Ercha et al., 2012; Yigit et al., 2016) have highlighted the enhanced interhemispherical asymmetries in Total Electron Content (TEC) and other thermospheric density, and composition changes during geomagnetic storms. However, the timescale of the instant response of the altitudinal variations in this event of 9 November 2004 is difficult to explain by any changes in thermospheric neutral winds. Another possibility is that the transmission of PP electric field from high to low latitudes is believed to be due to TMO propagation mode (Kikuchi et al., 1978), which has very weak latitudinal variation (Fejer et al., 1990), but it is not known if the overshielding field adopts a different mode of propagation which can produce stronger latitudinal differences. A third possible mechanism is that the location of R2 current system being more toward the equator, one can imagine that R2 current system (responsible for the overshielding effects) have smaller-scale size compared to that of R1 current system (associated with the undershielding penetration). It may be reasonable to anticipate that the systems with smaller-scale sizes can produce larger gradients compared to that of the larger size systems. Therefore, it is possible that the larger latitudinal gradients observed during overshielding are due to the smaller-scale size of R2 current system. The available data sets do not permit verification of these suggestions and calls for further investigations using coordinated measurements of ionospheric parameters and modeling. Nevertheless, the importance of these variations needs to be taken seriously to understand the 3-D ionospheric electrodynamic. It also needs to be investigated that whether such large altitudinal gradients are common during space weather events or they became pronounced because of the extreme nature of the studied event.

Thus, in short, the explanation of the observed variations of the vertical plasma drifts in the equatorial ionosphere can be sought through various schemes such as the modification of potential distribution by sudden withdrawal of PP electric field, dominance of overshielding field together with changes in convection of thermospheric winds, if any, different modes of propagation or difference in the scale sizes of the R1 and R2 current systems.

#### 4. Summary

The ionospheric  $F$  region response to the space weather event of 9 November 2004 is discussed in the light of altitudinal variations in vertical plasma transportation as observed by the Jicamarca ISR. When mostly

such variations are neglected, they reflect the latitudinal variations in low latitudes and can have significant control over the plasma transportation under different external drivers. It is shown that the  $F$  region responded differently under the influence of PP electric field and overshielding. The resultant field during overshielding period caused large altitudinal variations in the vertical plasma drifts. This would be expected to cause differential plasma movement in the  $F$  region topside and bottomside and will have a direct impact on satellite drag in the LEO orbits. Incorporating these altitudinal variations are important for three-dimensional electrodynamics models and are crucial to space weather predictions. It is demonstrated that the Jicamarca ISR can be used to continuously monitor and gain insight into such complex  $F$  region responses to different drivers. The results were compared with the simulation run using TIEGCM and USU-GAIM. It was found that when the magnitude of the drifts matched well with the observations, the model could not reproduce the differential response and altitudinal variations under the influence of overshielding field. We report here clear differences in the altitudinal gradients of the vertical drifts and hence the zonal electric fields during prompt penetration and overshielding conditions. This may indicate that the latitudinal gradients of the zonal electric fields are very small during prompt penetration and are quite significant during overshielding conditions. This triggers a very important question whether the propagation mechanisms of the electric fields from high to low latitudes during prompt penetration and overshielding conditions are the same or if they adopt different modes of propagation. Or else, are the observed larger latitudinal gradients during overshielding associated with the smaller-scale sizes of R2 current system than R1 currents?

#### Acknowledgments

The solar wind data and the geomagnetic indices data are taken from NASA OMNI CDA web (<http://cdaweb.gsfc.nasa.gov/>). The ISR drift data from the Peruvian sectors are taken from <http://jro.igpp.gov.pe/english/>. The Jicamarca Radio Observatory is a facility of the Instituto Geofísico del Perú operated with support from the NSF AGS-1433968 through Cornell University. The TIEGCM and USU-GAIM model run results are available in the public domain of the Community Coordinated Modeling Center website (<https://ccmc.gsfc.nasa.gov/>). D. H. thanks Ja Soon, A. M. Mendoza, and other staffs from CCMC for their patience and cooperation on troubleshooting crashed runs for the models. D. H. also thanks D. Singh for helping with APEX geomagnetic coordinate conversion using Richmond, A. D., (1995), Ionospheric Electrodynamics Using Magnetic Apex Coordinates, *J. Geomag. Geoelectr.*, 47, 191–212. This work is supported by the Department of Science and Technology, Government of India.

#### References

- Astafeyeva, E., Zakharenkova, I., & Alken, P. (2016). Prompt penetration electric fields and the extreme topside ionospheric response to the 22–23 June 2015 geomagnetic storm as seen by the Swarm constellation. *Earth, Planets and Space*, 68(1), 152. <https://doi.org/10.1186/s40623-016-0526-x>
- Astafeyeva, E., Zakharenkova, I., & Doornbos, E. (2015). Opposite hemispheric asymmetries during the ionospheric storm of 29–31 August 2004. *Journal of Geophysical Research: Space Physics*, 120, 697–714. <https://doi.org/10.1002/2014JA020710>
- Astafeyeva, E., Zakharenkova, I., & Förster, M. (2015). Ionospheric response to the 2015 St. Patrick's Day storm: A global multi-instrumental overview. *Journal of Geophysical Research: Space Physics*, 120, 9023–9037. <https://doi.org/10.1002/2015JA021629>
- Bhaskar, A., & Vichare, G. (2013). Characteristics of penetration electric fields to the equatorial ionosphere during southward and northward IMF turnings. *Journal of Geophysical Research: Space Physics*, 118, 4696–4709. <https://doi.org/10.1002/jgra.50436>
- Blanc, M., & Richmond, A. (1980). The ionospheric disturbance dynamo. *Journal of Geophysical Research*, 85(A4), 1669–1686. <https://doi.org/10.1029/JA085iA04p01669>
- Burke, W. J., Kelley, M. C., Sagalyn, R. C., Smiddy, M., & Lai, S. T. (1979). Polar cap electric field structures with a northward interplanetary magnetic field. *Geophysical Research Letters*, 6(1), 21–24. <https://doi.org/10.1029/GL006i001p00021>
- Bussy-Virat, C. D., Ridley, A. J., & Getchius, J. W. (2018). Effects of uncertainties in the atmospheric density on the probability of collision between space objects. *Space Weather*, 16, 519–537. <https://doi.org/10.1029/2017SW001705>
- Chakrabarty, D., Hui, D., Rout, D., Sekar, R., Bhattacharyya, A., Reeves, G. D., & Ruohoniemi, J. M. (2017). Role of IMF  $B_y$  in the prompt electric field disturbances over equatorial ionosphere during a space weather event. *Journal of Geophysical Research: Space Physics*, 122, 2574–2588. <https://doi.org/10.1002/2016JA022781>
- Crooker, N. U. (1992). Reversed convection. *Journal of Geophysical Research*, 97(A12), 19363. <https://doi.org/10.1029/92JA01532>
- Deng, Y., Lu, G., Kwak, Y.-S., Sutton, E., Forbes, J., & Solomon, S. (2009). Reversed ionospheric convections during the November 2004 storm: Impact on the upper atmosphere. *Journal of Geophysical Research*, 114, A07313. <https://doi.org/10.1029/2008JA013793>
- Dickinson, R. E., Ridley, E. C., & Roble, R. G. (1981). A three-dimensional general circulation model of the thermosphere. *Journal of Geophysical Research*, 86(A3), 1499–1512. <https://doi.org/10.1029/JA086iA03p01499>
- Eccles, J. V. (1998). Modeling investigation of the evening prereversal enhancement of the zonal electric field in the equatorial ionosphere. *Journal of Geophysical Research*, 103(A11), 26,709–26,719. <https://doi.org/10.1029/98JA02656>
- Ercha, A., Ridley, A. J., Zhang, D., & Xiao, Z. (2012). Analyzing the hemispheric asymmetry in the thermospheric density response to geomagnetic storms. *Journal of Geophysical Research*, 117, A08317. <https://doi.org/10.1029/2011JA017259>
- Fejer, B. G. (1986). Equatorial ionospheric electric fields associated with magnetospheric disturbances. In Y. Kamide & J. A. Slavin (Eds.), *Solar Wind-Magnetosphere Coupling* (pp. 519–545). Tokyo: Terra Sci. [https://doi.org/10.1007/978-94-009-4722-1\\_37](https://doi.org/10.1007/978-94-009-4722-1_37)
- Fejer, B. G. (1991). Low latitude electrodynamic plasma drifts: A review. *Journal of Atmospheric and Terrestrial Physics*, 53(8), 677–693. [https://doi.org/10.1016/0021-9169\(91\)90121-M](https://doi.org/10.1016/0021-9169(91)90121-M)
- Fejer, B. G. (1997). The electrodynamic of the low-latitude ionosphere: Recent results and future challenges. *Journal of Atmospheric and Solar - Terrestrial Physics*, 59, 1456–1482. [https://doi.org/10.1016/S1364-6826\(96\)00149-6](https://doi.org/10.1016/S1364-6826(96)00149-6)
- Fejer, B. G. (2011). Low latitude ionospheric electrodynamic. *Space Science Reviews*, 158(1), 145–166. <https://doi.org/10.1007/s11214-010-9690-7>
- Fejer, B. G., Blanc, M., & Richmond, A. D. (2017). Post-storm middle and low-latitude ionospheric electric fields effects. *Space Science Reviews*, 206(1–4), 407–429. <https://doi.org/10.1007/s11214-016-0320-x>
- Fejer, B. G., Hui, D., Chau, J. L., & Kudeki, E. (2014). Altitudinal dependence of evening equatorial F region vertical plasma drifts. *Journal of Geophysical Research: Space Physics*, 119, 5877–5890. <https://doi.org/10.1002/2014JA019949>
- Fejer, B. G., Jensen, J. W., Kikuchi, T., Abdu, M. A., & Chau, J. L. (2007). Equatorial ionospheric electric fields during the November 2004 magnetic storm. *Journal of Geophysical Research*, 112, A10304. <https://doi.org/10.1029/2007JA012376>
- Fejer, B. G., Jensen, J. W., & Su, S.-Y. (2008a). Seasonal and longitudinal dependence of equatorial disturbance vertical plasma drifts. *Geophysical Research Letters*, 35, L20106. <https://doi.org/10.1029/2008GL035584>

- Fejer, B. G., Jensen, J. W., & Su, S.-Y. (2008b). Quiet time equatorial  $F$  region vertical plasma drift model derived from ROCSAT-1 observations. *Journal of Geophysical Research*, *113*, A05304. <https://doi.org/10.1029/2007JA012801>
- Fejer, B. G., Spiro, R. W., Wolf, R. A., & Foster, J. C. (1990). Latitudinal variation of perturbation electric fields during magnetically disturbed periods: 1986 SUNDIAL observation and model results. *Annales de Geophysique*, *8*, 441.
- Fesen, C., Crowley, G., Roble, R., Richmond, A. D., & Fejer, B. (2000). Simulation of pre-reversal enhancement on the low latitude vertical ion drifts. *Geophysical Research Letters*, *27*(13), 1851–1854. <https://doi.org/10.1029/2000GL000061>
- Gonzales, C. A., Kelley, M. C., Fejer, B. G., Vickrey, J. F., & Woodman, R. F. (1979). Equatorial electric fields during magnetically disturbed conditions 2. Implications of simultaneous auroral and equatorial measurements. *Journal of Geophysical Research*, *84*, 5803.
- Hagan, M. E., & Forbes, J. M. (2002). Migrating and nonmigrating diurnal tides in the middle and upper atmosphere excited by tropospheric latent heat release. *Journal of Geophysical Research*, *107*(D24), 4754. <https://doi.org/10.1029/2001JD001236>
- Hagan, M. E., Maute, A., Roble, R. G., Richmond, A. D., Immel, T. J., & England, S. L. (2007). Connections between deep tropical clouds and the Earth's ionosphere. *Geophysical Research Letters*, *34*, L20109. <https://doi.org/10.1029/2007GL030142>
- Heelis, R. A., Lowell, J. K., & Spiro, R. W. (1982). A model of the high-latitude ionospheric convection pattern. *Journal of Geophysical Research*, *87*(A8), 6339–6345. <https://doi.org/10.1029/JA087iA08p06339>
- Huang, C.-S., Yumoto, K., Abe, S., & Sofko, G. (2008). Low-latitude ionospheric electric and magnetic field disturbances in response to solar wind pressure enhancements. *Journal of Geophysical Research*, *113*, A08314. <https://doi.org/10.1029/2007JA012940>
- Hui, D., Chakrabarty, D., Sekar, R., Reeves, G. D., Yoshikawa, A., & Shiokawa, K. (2017). Contribution of storm time substorms to the prompt electric field disturbances in the equatorial ionosphere. *Journal of Geophysical Research: Space Physics*, *122*, 5568–5578. <https://doi.org/10.1002/2016JA023754>
- Hui, D., & Fejer, B. G. (2015). Daytime plasma drifts in the equatorial lower ionosphere. *Journal of Geophysical Research: Space Physics*, *120*, 9738–9747. <https://doi.org/10.1002/2015JA021838>
- Kelley, M. C., Makela, J. J., Chau, J. L., & Nicolls, M. J. (2003). Penetration of the solar wind electric field into the magnetosphere/ionosphere system. *Geophysical Research Letters*, *30*(4), 1158. <https://doi.org/10.1029/2002GL016321>
- Kikuchi, T., Araki, T., Maeda, H., & Maekawa, K. (1978). Transmission of polar electric fields to the equator. *Nature*, *30*(4), 650–651. <https://doi.org/10.1029/2002GL016321>
- Kikuchi, T., Luhr, H., Kitamura, T., Saka, O., & Schlegel, K. (1996). Direct penetration of the polar electric field to the equator during a DP2 event as detected by the auroral and equatorial magnetometer chains and the EISCAT radar. *Journal of Geophysical Research*, *101*, 19,643.
- Killeen, T. L., Heelis, R. A., Hays, P. B., Spencer, N. W., & Hanson, W. B. (1985). Neutral motions in the polar thermosphere for northward interplanetary magnetic field. *Geophysical Research Letters*, *12*(4), 159–162. <https://doi.org/10.1029/GL012i004p00159>
- Kudeki, E., Bhattacharyya, S., & Woodman, R. F. (1999). A new approach in incoherent scatter  $F$  region  $E \times B$  drift measurements at Jicamarca. *Journal of Geophysical Research*, *104*(A12), 28,145–28,162. <https://doi.org/10.1029/1998JA900110>
- Liu, H.-L., Yudin, V. A., & Roble, R. G. (2013). Day-to-day ionospheric variability due to lower atmosphere perturbations. *Geophysical Research Letters*, *40*, 665–670. <https://doi.org/10.1002/grl.50125>
- McLandress, C. M., Shepherd, G. G., & Solheim, B. H. (1996). Satellite observations of thermospheric tides: Results from the wind imaging interferometer on UARS. *Journal of Geophysical Research*, *101*(D2), 4093–4114. <https://doi.org/10.1029/95JD03359>
- Murphy, J. A., & Heelis, R. (1986). Implications on the relationship between electromagnetic drift components at mid and low latitudes. *Planetary and Space Science*, *34*(7), 645–652. [https://doi.org/10.1016/0032-0633\(86\)90042-5](https://doi.org/10.1016/0032-0633(86)90042-5)
- Nicolls, M. J., Kelley, M. C., Chau, J. L., Veliz, O., Anderson, D., & Anghel, A. (2007). The spectral properties of low latitude daytime electric fields inferred from magnetometer observations. *Journal of Atmospheric and Terrestrial Physics*, *69*(10–11), 1160–1173. <https://doi.org/10.1016/j.jastp.2006.08.015>
- Nishida, A. (1968). Coherence of geomagnetic DP 2 fluctuations with interplanetary magnetic variations. *Journal of Geophysical Research*, *73*(17), 5549–5559. <https://doi.org/10.1029/JA073i017p05549>
- Nopper, R. W., & Carovillano, R. L. (1978). Polar-equatorial coupling during magnetically active periods. *Geophysical Research Letters*, *5*(8), 699–702. <https://doi.org/10.1029/GL005i008p00699>
- Patra, A. K., Chaitanya, P. P., Otsuka, Y., Yokoyama, T., Yamamoto, M., Stoneback, R. A., & Heelis, R. A. (2014). Vertical  $E \times B$  drifts from radar and C/NOFS observations in the Indian and Indonesian sectors: Consistency of observations and model. *Journal of Geophysical Research: Space Physics*, *119*, 3777–3788. <https://doi.org/10.1002/2013JA019732>
- Pedatella, N. M., Lei, J., Larson, K. M., & Forbes, J. M. (2009). Observations of the ionospheric response to the 15 December 2006 geomagnetic storm: Long-duration positive storm effect. *Journal of Geophysical Research*, *114*, A12313. <https://doi.org/10.1029/2009JA014568>
- Pingree, J. E., & Fejer, B. G. (1987). On the height variation of the equatorial  $F$  region vertical plasma drifts. *Journal of Geophysical Research*, *92*(A5), 4763–4766. <https://doi.org/10.1029/JA092iA05p04763>
- Qian, L., Burns, A. G., Emery, B. A., Foster, B., Lu, G., Maute, A., et al. (2014). The NCAR TIE-GCM. In J. Huba, R. Schunk, & G. Khazanov (Eds.), *Modeling the ionosphere-thermosphere system* (Chap. 7, pp. 73–84). <https://doi.org/10.1002/9781118704417.ch7>
- Qian, L., Solomon, S. C., & Kane, T. J. (2009). Seasonal variation of thermospheric density and composition. *Journal of Geophysical Research*, *114*, A01312. <https://doi.org/10.1029/2008JA013643>
- Richmond, A. D., Peymirat, C., & Roble, R. G. (2003). Long-lasting disturbances in the equatorial ionospheric electric field simulated with a coupled magnetosphere-ionosphere-thermosphere model. *Journal of Geophysical Research*, *108*(A3), 1118. <https://doi.org/10.1029/2002JA009758>
- Richmond, A. D., Ridley, E. C., & Roble, R. G. (1992). A thermosphere/ionosphere general circulation model with coupled electro-dynamics. *Geophysical Research Letters*, *19*(6), 601–604. <https://doi.org/10.1029/92GL00401>
- Ridley, A. J., Lu, G., Clauer, C. R., & Papitashvili, V. O. (1998). A statistical study of the ionospheric convection response to changing interplanetary magnetic field conditions using the assimilative mapping of ionospheric electro-dynamics technique. *Journal of Geophysical Research*, *103*(A3), 4023–4039. <https://doi.org/10.1029/97JA03328>
- Rishbeth, H. (1977). Drifts and winds in the polar  $F$  region. *Journal of Atmospheric and Terrestrial Physics*, *39*(1), 111–116. [https://doi.org/10.1016/0021-9169\(77\)90051-4](https://doi.org/10.1016/0021-9169(77)90051-4)
- Roble, R. G., Ridley, E. C., Richmond, A. D., & Dickinson, R. E. (1988). A coupled thermosphere/ionosphere general circulation model. *Geophysical Research Letters*, *15*(12), 1325–1328. <https://doi.org/10.1029/GL015i012p01325>
- Sastri, J. H. (1988). Equatorial electric fields of the disturbance dynamo origin. *Annales de Geophysique*, *6*, 635.
- Scherliess, L., & Fejer, B. G. (1999). Radar and satellite global equatorial  $F$  region vertical drift model. *Journal of Geophysical Research*, *104*(A4), 6829–6842. <https://doi.org/10.1029/1999JA900025>

- Scherliess, L., Schunk, R. W., Sojka, J. J., Thompson, D. C., & Zhu, L. (2006). Utah State University global assimilation of ionospheric measurements gauss-Markov Kalman filter model of the ionosphere: Model description and validation. *Journal of Geophysical Research*, *111*, A11315. <https://doi.org/10.1029/2006JA011712>
- Schunk, R. W., Scherliess, L., Sojka, J. J., Thompson, D. C., Anderson, D. N., Codrescu, M., et al. (2004). Global assimilation of ionospheric measurements (GAIM). *Radio Science*, *39*, RS1S02. <https://doi.org/10.1029/2002RS002794>
- Song, P., Russell, C. T., Elphic, R. C., Gosling, J. T., & Cattell, C. A. (1990). Structure and properties of the subsolar magnetopause for northward IMF: ISEE observations. *Journal of Geophysical Research*, *95*(A5), 6375. <https://doi.org/10.1029/JA095iA05p06375>
- Tsurutani, B., Mannucci, A., Iijima, B., Ali, M., Jose, A., Sobral, H. A., et al. (2004). Global dayside ionospheric uplift and enhancement associated with interplanetary electric fields. *Journal of Geophysical Research*, *109*, A08302. <https://doi.org/10.1029/2003JA010342>
- Tsurutani, B. T., Echer, E., Guarnieri, F. L., & Kozyra, J. U. (2008). CAWSES November 7–8, 2004, superstorm: Complex solar and interplanetary features in the post-solar maximum phase. *Geophysical Research Letters*, *35*, L06S05. <https://doi.org/10.1029/2007GL031473>
- Tsurutani, B. T., Verkhoglyadova, O. P., Mannucci, A. J., Araki, T., Saito, A., Tsuda, T., & Yumoto, K. (2007). Oxygen ion uplift and satellite drag effects during the 30 October 2003 daytime superfountain event. *Annales de Geophysique*, *25*(3), 569–574. <https://doi.org/10.5194/angeo-25-569-2007>
- Vichare, G., & Richmond, A. D. (2005). Simulation study of the longitudinal variation of evening vertical ionospheric drifts at the magnetic equator during equinox. *Journal of Geophysical Research*, *110*, A05304. <https://doi.org/10.1029/2004JA010720>
- Weimer, D. R. (2005). Improved ionospheric electrodynamic models and application to calculating joule heating rates. *Journal of Geophysical Research*, *110*, A05306. <https://doi.org/10.1029/2004JA010884>
- Wolf, R. A. (1983). The quasi-static (slow flow) region of the magnetosphere. In R. L. Carovillano & J. M. Forbes (Eds.), *Solar Terrestrial Physics* (pp. 303–368). Hingham, MA: D. Reidel.
- Yigit, E., Frey, H. U., Moldwin, M. B., Immel, T. J., & Ridley, A. J. (2016). Hemispheric differences in the response of the upper atmosphere to the August 2011 geomagnetic storm: A simulation study. *Journal of Atmospheric and Solar - Terrestrial Physics*, *141*, 13–26. <https://doi.org/10.1016/j.jastp.2015.10.002>
- Yizengaw, E., Moldwin, M. B., Komjathy, A., & Mannucci, A. J. (2006). Unusual topside ionospheric density response to the November 2003 superstorm. *Journal of Geophysical Research*, *111*, A02308. <https://doi.org/10.1029/2005JA011433>
- Zhang, R., Liu, L., Le, H., Chen, Y., & Kuai, J. (2017). The storm time evolution of the ionospheric disturbance plasma drifts. *Journal of Geophysical Research: Space Physics*, *122*, 11,665–11,676. <https://doi.org/10.1002/2017JA024637>